



# The Role of Acetylation and Methylation of Rat Hippocampal Histone H3 in the Mechanism of Aluminum-Induced Neurotoxicity

Jie Gao<sup>1</sup> · Wei Liu<sup>1</sup> · Jiaqi Liu<sup>1</sup> · Niping Hao<sup>1</sup> · Jing Pei<sup>1</sup> · Lifeng Zhang<sup>1</sup>

Received: 15 June 2023 / Revised: 9 October 2023 / Accepted: 14 October 2023

© The Author(s), under exclusive licence to Springer Science+Business Media, LLC, part of Springer Nature 2023

## Abstract

Aluminum is a known neurotoxin and a major environmental contributor to neurodegenerative diseases such as Alzheimer's disease (AD). We used a subchronic aluminum chloride exposure model in offspring rats by continuously treating them with AlCl<sub>3</sub> solution from the date of birth until day 90 in this research. Then evaluated the neurobehavioral changes in rats, observed the ultrastructural changes of hippocampal synapses and neurons, and examined the level of hippocampal acetylated histone H3 (H3ac), the activity and protein expression of hippocampal HAT1 and G9a, and the protein expression level of H3K9 dimethylation (H3K9me2). The findings demonstrated that aluminum-treated offspring rats had impaired learning and memory abilities as well as ultrastructural alterations in hippocampal synapses and neurons. The level of histone H3ac was decreased along with decreased protein expression and activity of HAT1, while level of H3K9me2 was increased along with increased protein expression and activity of G9a.

**Keywords** Aluminum · Hippocampus · Neurotoxicity · Histone H3 · Acetylation · Methylation · Epigenetics

## Introduction

Aluminum (Al) is a light metal, and its compounds are extremely widely distributed in nature, occurring in air, water, and food. A acceptable weekly consumption of 1 mg/kg of Al has been defined by the European Food Safety Authority (EFSA) [1], which may be obtained from food exposure alone, and Al exposure has become a growing public health concern [2]. The blood levels, musculoskeletal system, kidneys, liver, respiration, and neurological system can all be impacted by Al treatment [3]. Al is an identified neurotoxin that can destroy the blood-brain barrier and accumulate in hippocampal tissue for long periods of time, and is concerned with neuroinflammation, dysmnnesia, and neurological disorders through various mechanisms [4]. The hippocampus is the “flash drive” of the human brain and is often associated with memory consolidation

and decision-making, but it is far more complex in structure and function than a flash drive. The hippocampus has three distinct zones: the dentate gyrus, the hippocampus proper, and the subiculum. The Cornu Ammonis (CA) is a structure similar to a seahorse or ram's horn that describes the different layers of the hippocampus. The hippocampal region has four subregions: CA1, CA2, CA3, and CA4 (often referred to as the hilus region and considered part of the dentate gyrus). The sides of CA3 and CA2 border the ridges of the dentate gyrus, and CA3 is the largest in the hippocampus [5–7]. Hippocampal CA3 is currently considered to be one of the major brain regions involved in learning, memory, and cognitive performance [8].

The neurotoxicity mechanism of Al is complicated, and numerous epigenetic alterations may be one of the significant causes of cognitive decline brought by Al. Epigenetics refers to heritable changes caused by altered gene expression without alteration in DNA sequence, and the majority of studies on Al neurotoxicity at the moment focus on DNA methylation modification and post-translational modifications of histones [9, 10]. Histone modifications control the transcription of plasticity genes, modify individual neuronal responses, and play a crucial role in memory storage and consolidation. The degree of histone acetylation, which is controlled by histone acetyltransferases (HATs)

Jie Gao and Wei Liu contributed equally to this work.

✉ Lifeng Zhang  
zgykdxzlf@163.com

<sup>1</sup> Department of Maternal, Child and Adolescent Health, School of Public Health, Shenyang Medical College, Shenyang 110034, Liaoning Province, P. R. China

and histone deacetylases (HDACs) among these modifications, is essential to regulate gene transcription and expression. One of the most well researched mechanisms in the numerous types of histone modification is histone acetylation, which frequently takes place on amino acid residues at the ends of histone H3 or H4 and has the role of activating transcription and increasing gene expression [11]. HATs are widely present in many tissues and organs and can mediate the addition of acetyl groups to amino acid residues at the ends of histone subunits, raise histone acetylation levels, activate particular genes and hence increasing transcription [12]. Our earlier research has demonstrated that exposure to AI can decrease the level of acetylated histone H4 by raising the production of the HDAC2 gene and protein expression, which impairs rats' capacity for learning and memory [13].

The methylation of the histone protein lysine is crucial for brain development and memory formation and maintenance, it is the molecular basis of chromosome function both inside and outside the body. Studies have shown increased dimethylation of lysine 9 in histone H3 in an animal model of age-related memory impairment [14]. The heterodimer complex formed by the histone lysine methyltransferase G9a is capable of monomethylating and dimethylating the N-terminal tail of histone H3K9, which inhibits transcription [15].

However, whether AI exerts neurotoxic effects by altering epigenetic states remains largely unknown. Then, may AI have an impact on HAT1 and G9a activity, affecting histone H3ac and H3K9me2 in the process and contributing to the molecular mechanism of AI-induced learning and memory impairment? This study explored the possibility of histone H3 as a neurotoxic potential treatment target for AI from an epigenetic perspective by establishing a subchronic AI exposure model for the offspring of rats, providing new insights into the pathogenic mechanisms and preventive approaches to neurodegenerative diseases.

## Materials and Methods

### Chemicals

AlCl<sub>3</sub>·6H<sub>2</sub>O (Sinopharm Chemical Reagents Co., China); SP method immunohistochemistry kit, DAB color development kit (Maxim biotechnologies Co., China); Embedding machine and paraffin sectioning machine (Leica Co., Germany); Rabbit anti-acetylated histone H3 antibody (Sanying biotechnology Co., China); Rabbit anti-G9a, H3K9me2 antibody (Abcam Co., UK); Rabbit anti-HAT1, β-actin antibody, Horseradish peroxidase-labeled sheep anti-rabbit IgG antibody (ABclonal Co., China); Nucleoprotein and cytoplasmic protein extraction kit, BCA protein content

detection kit (Keygentec Co., China); Tween, Tris, Glycine, Sodium dodecyl sulfate SDS (Solarbio Co., China); SDS-PAGE gel kit, SDS-PAGE protein loading buffer (Beyotime Co., China); HAT1 ELISA Kit (Boster Co., China); G9a ELISA Kit (Mlbio Co., China); Anhydrous ethanol, xylene, methanol, nitric acid, hydrochloric acid (XiLong Co., China).

### Animals and AI Exposure Methods

Healthy and matured Wistar rats, weighing 220 ± 10 g, with 40 females and 20 males, were selected by the experimental animal center belonging to Shenyang Medical College. The rats were fed in a clean animal room with light and dark cycles for 12 h, the temperature was 20~24 °C, the humidity was 45~55%, and a free drinking water diet. The study followed guidelines for experimental animal management and experimental protocols were approved by the Medical Animal Ethics Committee of Shenyang Medical College.

Formal experimentation after 3 days of environmental adaptive feeding. On the basis of the World Health Organization's recommendation, the minimum allowable exposure to AI per week is 1 mg/kg [1] and the safety factor between human and animals is 100 times, which is exchanged for the low toxic dosage for rats, and is gradually increased by 2 times for the medium and high toxic dose group. By random number table method, female rats were divided into three dose groups and control group according to body weight, 10 per group. Female: Male = 2:1 cage mating. In the next morning, observation of vaginal suppository or colposcopy of sperm was considered to be pregnant, pregnant rats were routinely fed until delivery. Pregnant rats were contaminated with AI on the first day (Day 0) of delivery. During lactation, female rats in different dosage groups were given distilled water solution containing AlCl<sub>3</sub> concentration of 0, 2.0, 4.0, 8.0 g/L, respectively, and their offspring were poisoned through milk. At the end of the lactation period, the offspring rats individually drank distilled water solutions containing different dosages of AlCl<sub>3</sub>. Simulating the AI exposure of human babies from lactation to adulthood, the period of exposure lasted 90 days from the first day of birth in rats. During the experiment, the weight of the rats in different dosage groups was regularly weighed weekly, and the consumption of water and feed, mental state, hair and overall condition of the rats were observed. According to the results of the observational measurement, the average water intake of rats in each group was relatively constant, so the AI intake was consistent with the experimental design.

## Morris Water Maze (MWM)

Eight rats in different dosage groups were randomly chosen (female: male = 1:1) for the MWM experiment 24 h after the end of the last Al exposure. During the experiment, the water temperature was retained at  $22 \pm 2$  °C and the surrounding environment was steady, and the rats were permitted to swim optionally in the water for 2 min to familiarize with the circumstance before the formal experiment. The first 5 days of the positioning navigation experiment, the rats were randomly put into the water from 4 quadrants facing the wall of the pool every day, and the time to search the platform under the water surface (escape latency) was recorded, and the training duration was 120 s. After the positioning navigation test ended 24 h (Day 6), the space exploration experiment was started, the platform was removed, the rats were put into water in a random quadrant, and the residence time in the target quadrant and the platform crossing times in 120 s were recorded. These indicators were recorded by ANY-maze video tracking software (Stoelting Co., USA) and compared to analyze the performance of the rats.

## Shuttle Box Experiment

Eight rats (female: male = 1:1) in each group were randomly selected and placed in a shuttle box for 5 min, during which any activity was allowed to eliminate the exploratory reflex. In the shuttle box, the conditioned stimulation (bee sounds) was first given for 10 s, and then electrical stimulation (electric shock intensity of 30 V, 50 Hz) was applied simultaneously for 10 s. If the rats escaped to the safe area within 10 s of the light on, it was an active avoidance reaction; if the rat escaped to the safe area after electric shock, it was a passive avoidance reaction. After several training, the rats could gradually form the active avoidance conditioned response and thus acquire the memory. Each training 20 s, 20 cycles, consecutive 5 days. One week after the training, the same group of rats were carried out formal experiment in the shuttle box under the same time and environmental conditions. The number of shocks, duration of shocks and active avoidance latency were recorded to assess the active and passive avoidance response.

## ICP-MS

Brain tissue was dissected from rats after decapitation and six hippocampi per group were accurately weighed 0.2 g into the polytetrafluon digestion tube, and 5 mL of superior pure nitric acid and 1 mL of superior pure hydrochloric acid were added, sealed, and put into the porcelain tube for the digestion of tissues in the ultra-high pressure microwave digestion apparatus (Anton Paar Co., Austria) for about 1 h,

while blank control was performed. After the tissue was completely dissolved, the sample solution was transferred to a 50 mL volumetric bottle with 20% nitric acid, and the volume was fixed to 50 mL. The inductively coupled plasma mass spectrometer (Agilent Co., USA) was used to detect the Al content. The detected Al content was subtracted from the background value of the blank control to obtain the final Al ion content in the hippocampus of each rat.

## Transmission Electron Microscope Specimen Production

Eight rats in every group were randomly chosen, anesthetized with 1% sodium pentobarbital (40 mg/kg), and perfused with saline solution and 4 °C 2% paraformaldehyde-2.5% glutaraldehyde fixative (pH: 7.4) 100~150 ml for 20 min (first fast and then slow) before decapitation. The brain tissue was rapidly dissected on ice, submerged in 0 °C fixative for 24 h, and hippocampal tissue slices were excised in the horizontal coronal position of the lateral geniculate body, and 1 mm<sup>3</sup> tissue was taken from the CA3 region of the hippocampus. Fixed in 1% Osmium tetroxide, dehydrated, and embedded. The samples were then trimmed and cut into 70 µm slices, stained with saturated uranium acetate and lead citrate, and placed in clean petri dishes for spare. Finally, the ultrastructure of hippocampal synapses and neurons was observed under a transmission electron microscope (H-7650, Hitachi Co, Japan) at magnification 50000X.

## ELISA

ELISA was used to measure HAT1 and G9a enzyme activities in rat hippocampus. Eight hippocampal tissues were taken from each group, 0.05 g was weighed, 1 ml PBS was added, homogenized (80 Hz, 40 s), centrifuged at 3000 RPM/min for 20 min in a low temperature and high speed centrifuge (Sigma Co., Germany), and supernatant was collected. All operations were executed in strict accordance with the ELISA kit specification. Except for blank wells, each well was added with 100 µL enzyme-conjugate reagent, sealed with sealing plate film, and hatched at 37 °C for 60 min. Removed the sealing plate film, washed and dried, added color developing agent A and B 50 µL successively to every well, gently shaken and mixed, and developed color at 37 °C for 15 min. To end the reaction, 50 µL of termination solution were added to each well. Blank holes were zeroed, and absorbance (OD value) of every hole was determined successively at 450 nm wavelength, and the measurement should be initiated within 15 min after the termination solution was added. The linear regression equation of the standard curve was calculated using the standard concentration and OD value, and the sample OD value was

substituted into the equation to calculate the sample concentration, and then multiplied by the dilution times, which is the actual concentration of the sample, and the enzyme activity was expressed by the concentration.

### Immunohistochemical Method

Eight brain tissues of rats preserved in 4% paraformaldehyde were taken from each group, trimmed to exposed hippocampus, washed under running water overnight, dehydrated by gradient alcohol, dealcoholized by xylene, and then paraffin sections were prepared with a thickness of 4  $\mu\text{m}$  after conventional embedding. Before staining, the slices were roasted in HD-330 chip baking machine (Huida Instrument Co., China) at 70  $^{\circ}\text{C}$  for 1.5 h. The slices were dewaxed by xylene and dehydrated by gradient alcohol. 0.3%  $\text{H}_2\text{O}_2$  was added to the tissues, and rabbit anti-acetylated histone H3 antibody (dilution 1:150) and goat anti-rabbit IgG antibody labeled with horseradish peroxidase (dilution 1:2000) were added successively, and incubated at 4  $^{\circ}\text{C}$  overnight. After leaching in PBS, DAB color developing solution was added for 3 min, hematoxylin was re-dyed for 7 min, tap water was rinsed for 10 min, conventional gradient alcohol was dehydrated, xylene was dealcoholized, and neutral gum was sealed. At the same time, comparison was made under the same environment, observation was made under microscope (Leica Co., Germany) and photographs were taken. Image-Pro Plus 6.0 software was used to read the optical density of the protein expression region in the section photos, and Average optical density (AOD) and Integral optical density (IOD) were used to represent the expression level of acetylated histone H3.

### Western Blot

Eight hippocampi were taken from each group, 50 mg of hippocampal tissues were weighed, and tissue proteins were extracted according to the instructions of the nuclear

and cytoplasmic protein extraction kits. After quantitative analysis by BCA method, protein dilutions were made by adding protein loading buffer and  $\text{ddH}_2\text{O}$ . It was denatured by boiling at 100  $^{\circ}\text{C}$  for 7 min in Thermo Cell thermostatic metal bath and then stored at -80  $^{\circ}\text{C}$ . After 15% separation gel and 5% concentrated gel were prepared according to SDS-PAGE gel kit instructions, 10  $\mu\text{L}$  predictive protein solution was taken and subjected to 100 V constant pressure electrophoresis for 1.4 h in a protein electrophoresis facility (Bio-rad Co., USA), and transferred to a protein electro-printing facility (Bio-rad Co., USA) for 50 min at 100 V constant pressure. The protein was transferred to PVDF membrane and sealed with 5% skim milk for 2 h. Rabbit anti-HAT1, rabbit anti-G9a, rabbit anti-H3K9me2, and rabbit anti- $\beta$ -actin were added (dilutions 1:1000, 1:500, 1:500, 1:2000), and the mixture was incubated on a shaker for 1 h at 4  $^{\circ}\text{C}$  overnight. The next morning, the PVDF membrane was removed, and it was washed with PBST for 10 min and repeated 4 times. Then it was put into horseradish peroxidase-labeled goat anti-rabbit IgG antibody (1:10000) and hatched on a shaker for 1 h. The ECL reagent was developed, and the results were counted by the automatic chemiluminescence image analysis system (Tanon Technology Co., China). The grayscale values of the bands were scanned using Image J software, and the results were expressed as the grayscale values of the protein to be measured compared with the grayscale values of the  $\beta$ -actin bands.

### Statistical Analysis

The data was processed using SPSS 26.0, and the results were expressed in terms of mean  $\pm$  SD. One-way ANOVA was used for comparison between groups, and the LSD test was used if the variances were equal; if the variances were not equal, the Dunnett-t test was used. The repeated measures design information was compared using repeated measurement ANOVA. Pearson correlation coefficient ( $r$ ) was used to analyze the relevance. The test level was  $\alpha=0.05$ . Bar and line graphs were plotted using GraphPad Prism software.

## Result

### Basic Conditions of Rats During AI Exposure

There was no mortality in any group of rats during the drinking water exposure experiment. Hair, food, mental state, and free activity were all normal in the control group, while body weight increased as feeding time increased (Fig. 1). The rats in the 2.0 g/L and 4.0 g/L groups showed no obvious changes in body weight and mental state; the rats in

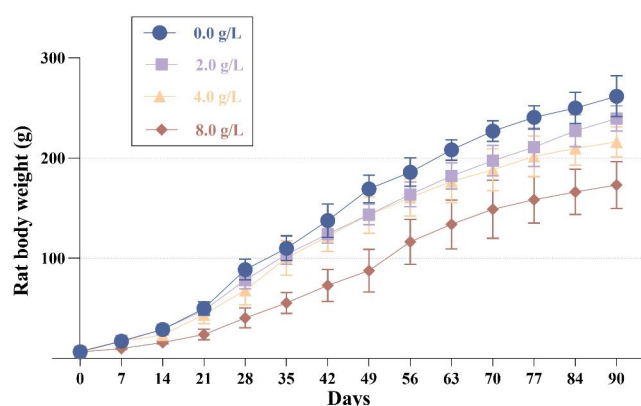
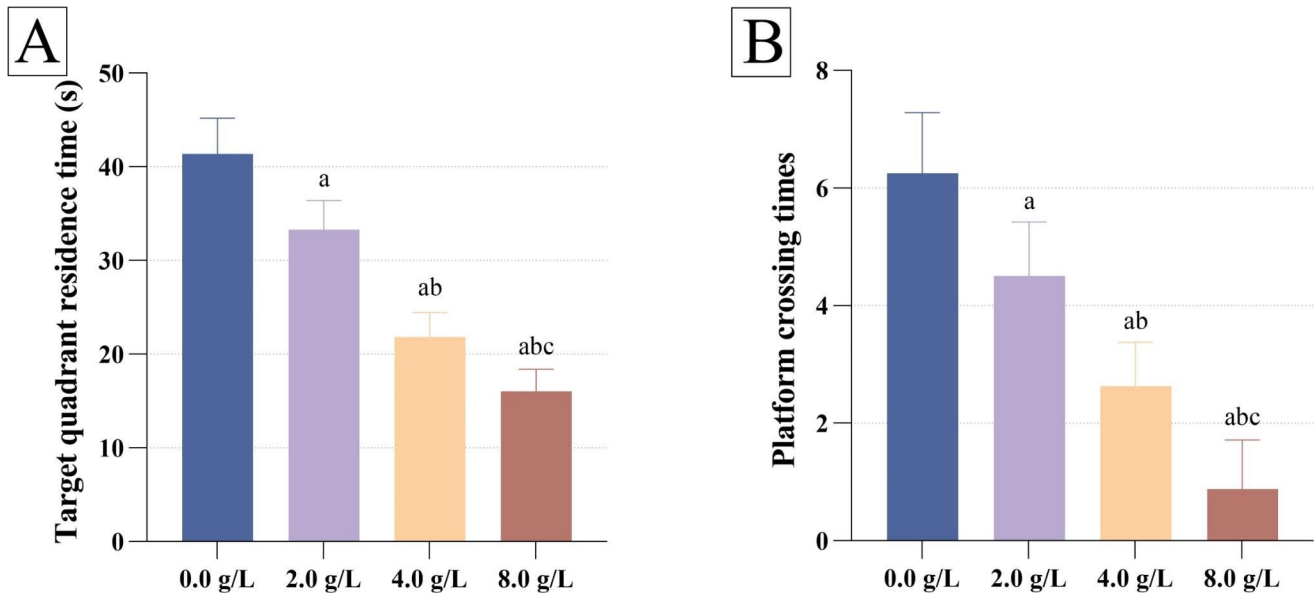


Fig. 1 Effects of AI on weight of rats (One-way ANOVA,  $n=8$ )

**Table 1** Comparison of escape latency in each group at different time points (mean  $\pm$  SD)

Group	Date				
	Day1	Day2	Day3	Day4	Day5
0.0 g/L	52.8 $\pm$ 6.5	29.9 $\pm$ 3.5 <sup>c</sup>	19.1 $\pm$ 2.6 <sup>c</sup>	16.0 $\pm$ 2.4 <sup>cde</sup>	9.1 $\pm$ 2.3 <sup>cdef</sup>
2.0 g/L	59.6 $\pm$ 4.5	34.8 $\pm$ 2.9 <sup>ac</sup>	27.4 $\pm$ 1.7 <sup>acd</sup>	22.0 $\pm$ 1.5 <sup>cde</sup>	17.9 $\pm$ 1.4 <sup>cdef</sup>
4.0 g/L	62.2 $\pm$ 3.6	43.0 $\pm$ 2.3 <sup>abc</sup>	33.3 $\pm$ 2.5 <sup>abcd</sup>	27.5 $\pm$ 1.1 <sup>abcde</sup>	21.9 $\pm$ 1.7 <sup>abcdef</sup>
8.0 g/L	72.4 $\pm$ 2.3	54.9 $\pm$ 2.7 <sup>abc</sup>	42.4 $\pm$ 4.2 <sup>abcd</sup>	31.4 $\pm$ 2.3 <sup>abcde</sup>	24.2 $\pm$ 2.2 <sup>abcdef</sup>

Note: <sup>a</sup> $P < 0.05$ , compared with 0.0 g/L at the same time point; <sup>b</sup> $P < 0.05$ , compared with 2.0 g/L at the same time point; <sup>c</sup> $P < 0.05$ , compared with the same group on Day 1; <sup>d</sup> $P < 0.05$ , compared with the same group on Day 2; <sup>e</sup> $P < 0.05$ , compared with the same group on Day 3; <sup>f</sup> $P < 0.05$ , compared with the same group on Day 4 (repeated measurement ANOVA,  $n = 8$ )



**Fig. 2** Comparison of Morris water maze space exploration experiment results in each group (One-way ANOVA,  $n = 8$ ). Note: <sup>a</sup> $P < 0.01$  vs. 0.0 g/L; <sup>b</sup> $P < 0.01$  vs. 2.0 g/L; <sup>c</sup> $P < 0.01$  vs. 4.0 g/L

the 8.0 g/L group showed different degrees of dark fur and mental depression, slow growth in body weight, slow reaction and reduced activity. The results of repeated analysis of variance showed that the weight of rats was statistically significant in the main effect of time, the interaction effect between dosage and time, and the main effect of dosage ( $F = 1921.43$ ,  $P < 0.05$ ;  $F = 14.23$ ,  $P < 0.05$ ;  $F = 60.93$ ,  $P < 0.05$ ).

### Subchronic AI Exposure Impaired Spatial Learning Memory

The results of positioning navigation experiment revealed that as training time increased, the escape latency of each group reduced. The escape latency of rats was statistically significant in the main effect of dosage, the main effect of time, and the interaction effect between dosage and time, ( $F = 322.96$ ,  $P < 0.05$ ;  $F = 1043.29$ ,  $P < 0.05$ ;  $F = 5.71$ ,  $P < 0.05$ ), and the analysis results of interaction effects are shown in Table 1.

In the space exploration experiment, the target quadrant residence time of rats in each dosage group was significantly different ( $F = 111.58$ ,  $P < 0.01$ ;  $r = -0.92$ ,  $P < 0.05$ ) in Fig. 2A. There was a significant difference in the number of times rats crossed the platform in each dosage group ( $F = 54.38$ ,  $P < 0.05$ ;  $r = -0.91$ ,  $P < 0.05$ ) in Fig. 2B.

The paths taken by the rats in each group to arrive the platform became increasingly obvious as the number of training days increased, while it in the AI-poisoned groups remained disordered (Fig. 3).

In the shuttle box test, the indexes of passive escape response: the number of electric shocks in rats differed between dosage groups ( $F = 39.95$ ,  $P < 0.05$ ;  $r = 0.83$ ,  $P < 0.05$ ) in Fig. 4A. The shock time of rats in each dosage group was significantly different ( $F = 44.62$ ,  $P < 0.05$ ;  $r = 0.90$ ,  $P < 0.05$ ) in Fig. 4B. Active escape indexes: the active escape time of rats differed between dosage groups ( $F = 53.18$ ,  $P < 0.05$ ;  $r = 0.92$ ,  $P < 0.05$ ) in Fig. 4C. The active escape latency of rats in each dosage group was significantly different ( $F = 31.25$ ,  $P < 0.05$ ;  $r = 0.87$ ,  $P < 0.05$ ) in Fig. 4D.

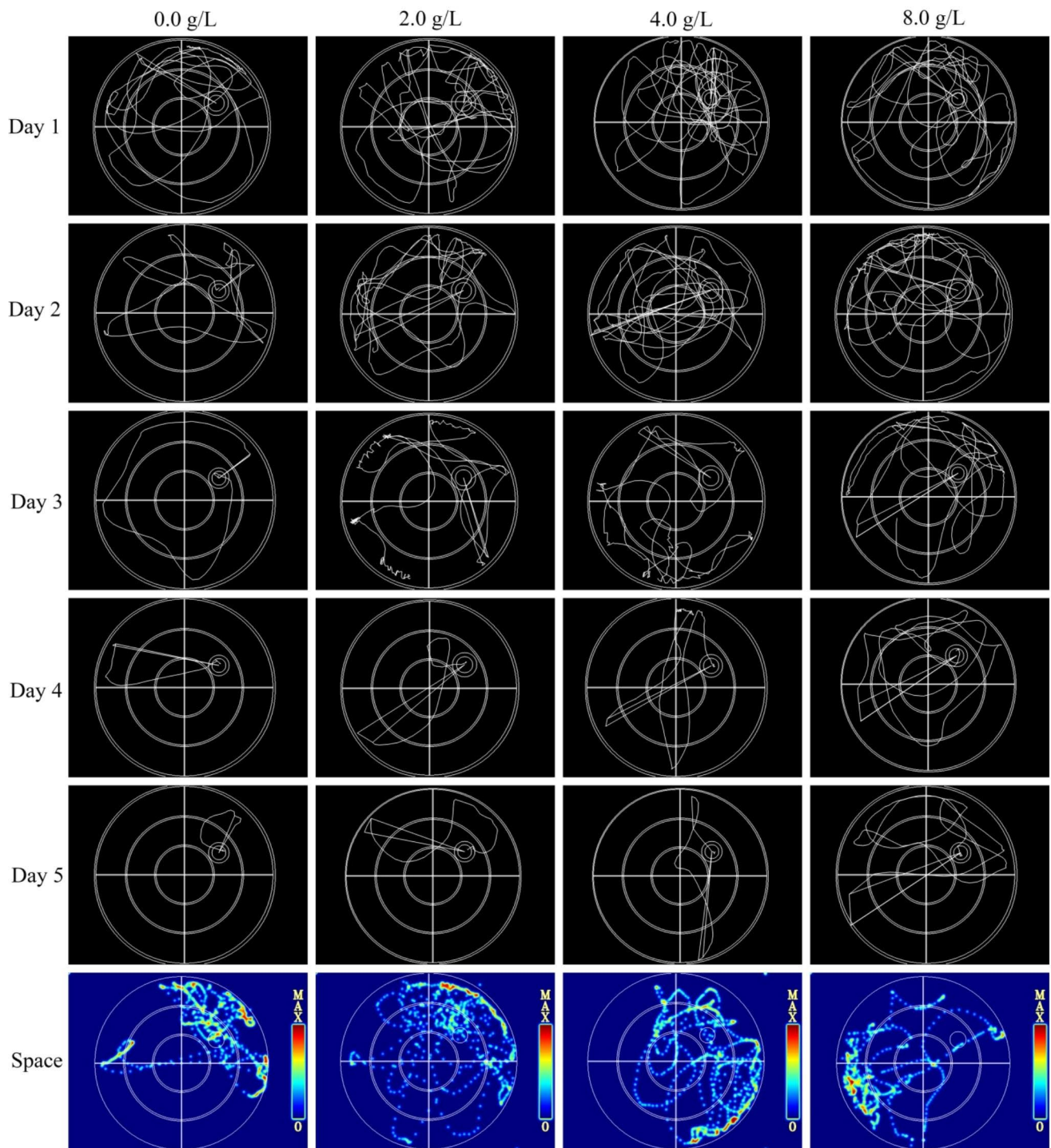


**Fig. 3** Pathway and hot spot map of the Morris water maze experiment for each group of rats

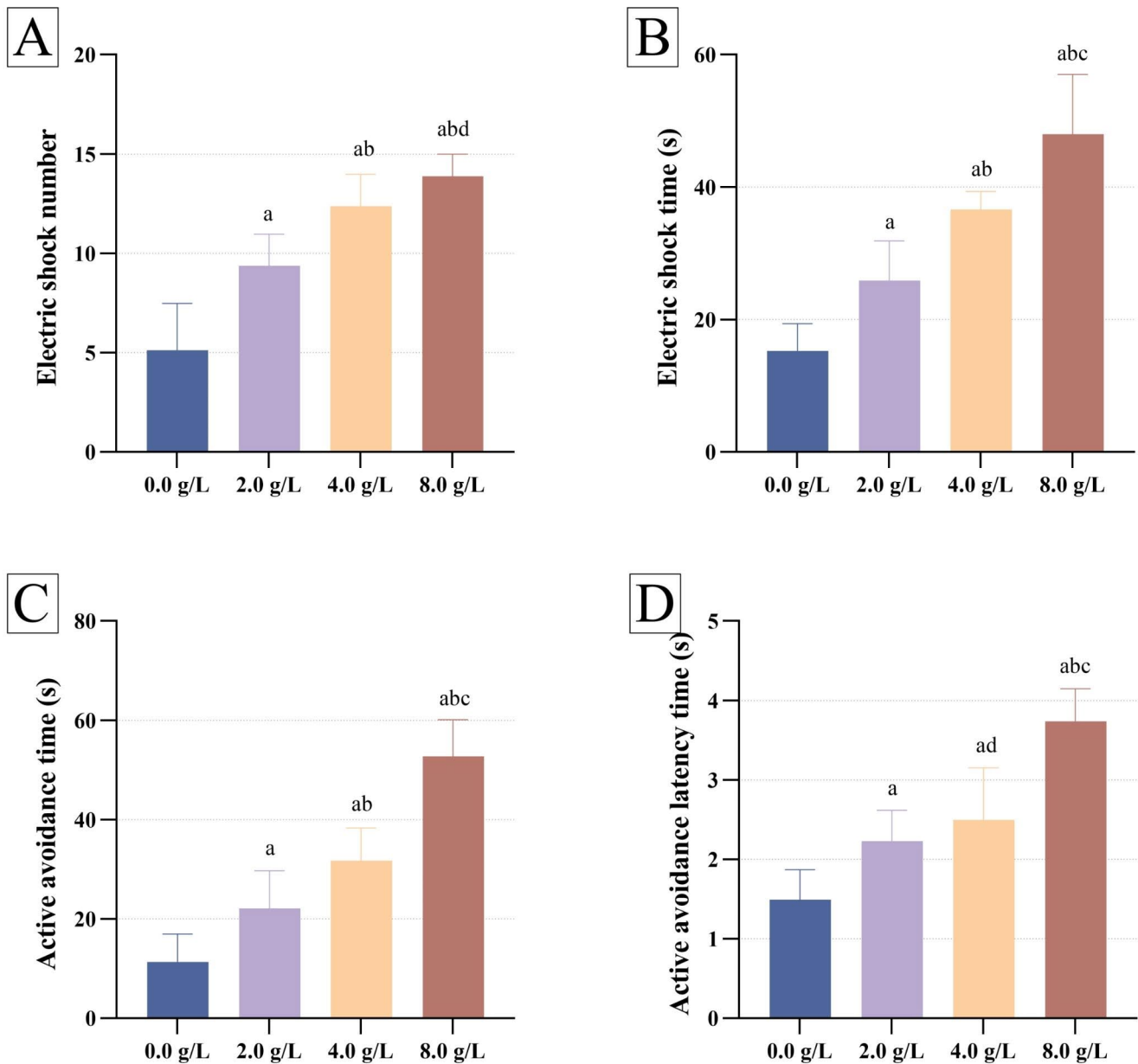


**Fig. 4** Analysis of shuttle box experiment results (One-way ANOVA,  $n = 8$ ). Note: <sup>a</sup> $P < 0.01$  vs. 0.0 g/L; <sup>b</sup> $P < 0.01$  vs. 2.0 g/L; <sup>c</sup> $P < 0.01$  vs. 4.0 g/L; <sup>d</sup> $P > 0.05$  vs. 2.0 g/L

### Subchronic Al Exposure Increased Al Content

Al was present in the hippocampus as  $Al^{3+}$ , and the Al content in each dosage group was measured using ICP-MS. The hippocampal Al content was higher in all three poisoned groups than in the control group, with statistically significant ( $F = 25.05$ ,  $P < 0.05$ ;  $r = 0.89$ ,  $P < 0.05$ ) in Fig. 5.

### Subchronic Al Exposure Disrupted the Ultrastructure of Neurons and Synapses

Figure 6 showed the ultrastructural changes of neurons and synapses in hippocampal CA3 region of rats in each group. As shown in the figure, the ultrastructural damage of neurons and synapses became more and more obvious with the increase of Al dose. The neurons in the 0.0 g/L group had abundant euchromatin, more rough endoplasmic reticulum and mitochondria in the cytoplasm, larger nuclei, obvious nuclear membranes and nucleolus. In the Al-exposed groups, neuron atrophy, cytoplasm concentration, mitochondrial

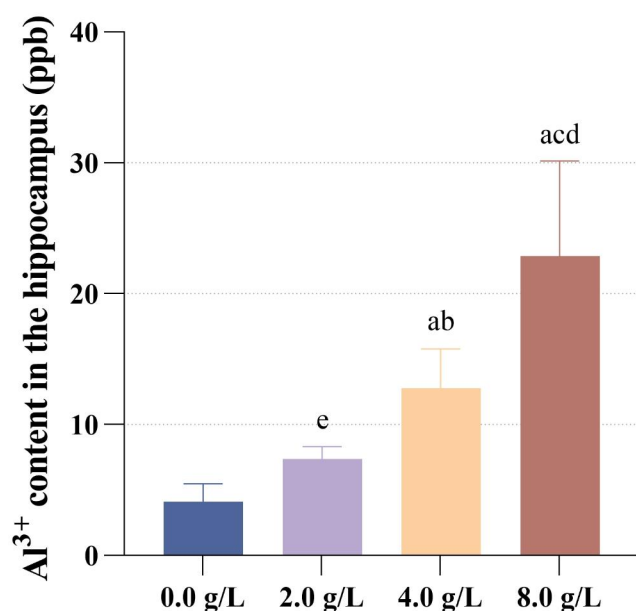


**Fig. 5** Al content in hippocampus of rats in each group (One-way ANOVA,  $n=6$ ). Note: <sup>a</sup> $P < 0.01$  vs. 0.0 g/L; <sup>b</sup> $P < 0.05$  vs. 2.0 g/L; <sup>c</sup> $P < 0.01$  vs. 2.0 g/L; <sup>d</sup> $P < 0.01$  vs. 4.0 g/L; <sup>e</sup> $P > 0.05$  vs. 0.0 g/L

swelling, cristae disturbance or disappearance, rough endoplasmic reticulum expansion, and extensive granular vacuolar degeneration (GVD) were observed, and the positive rate of GVD cells was positively correlated with the dose of Al. In the control group, hippocampal synapses were normal, but in the Al-exposed groups, the synaptic gaps were widened, the number of synaptic vesicles was reduced, the electron density of synapses was significantly increased, the anterior and posterior synaptic membranes were even fused and adhered, and myelin-like changes appeared in

the presynaptic membrane, which were formed after the destruction of mitochondria and rough endoplasmic reticulum. The arrangement of microfilament microtubules within the axon was disturbed, and even fracture, dissolution, and disappearance occurred.

### Changes of HAT1 and G9a Enzyme Activities

The ELISA results showed that the G9a enzyme activity in the hippocampus increased in each dosage group, with statistically significant ( $F = 135.13$ ,  $P < 0.05$ ;  $r = 0.95$ ,  $P < 0.05$ ) in Fig. 7A. The HAT1 enzyme activity was decreasing in each dosage group, with statistically significant ( $F = 28.08$ ,  $P < 0.05$ ;  $r = -0.84$ ,  $P < 0.05$ ) in Fig. 7B.

### Changes of HAT1, G9a, and H3K9me2 Protein Expression

The grayscale of HAT1, G9a, and H3K9me2 protein bands were used to indicate the relative expression of the corresponding proteins compared with the grayscale of  $\beta$ -actin protein bands. The results showed that G9a and H3K9me2 protein expression increased sequentially in each dosage group, with statistically significant ( $F = 18.31$ ,  $P < 0.05$ ;  $F = 45.00$ ,  $P < 0.05$ ) in Fig. 8A, B. There was a positive relevance between G9a and H3K9me2 protein expression and Al dosage, respectively ( $r = 0.84$ ,  $P < 0.05$ ;  $r = 0.94$ ,  $P < 0.05$ ). HAT1 protein expression in each dosage group decreased successively ( $F = 9.30$ ;  $P < 0.05$ ;  $r = -0.65$ ,  $P < 0.05$ ) in Fig. 8C.

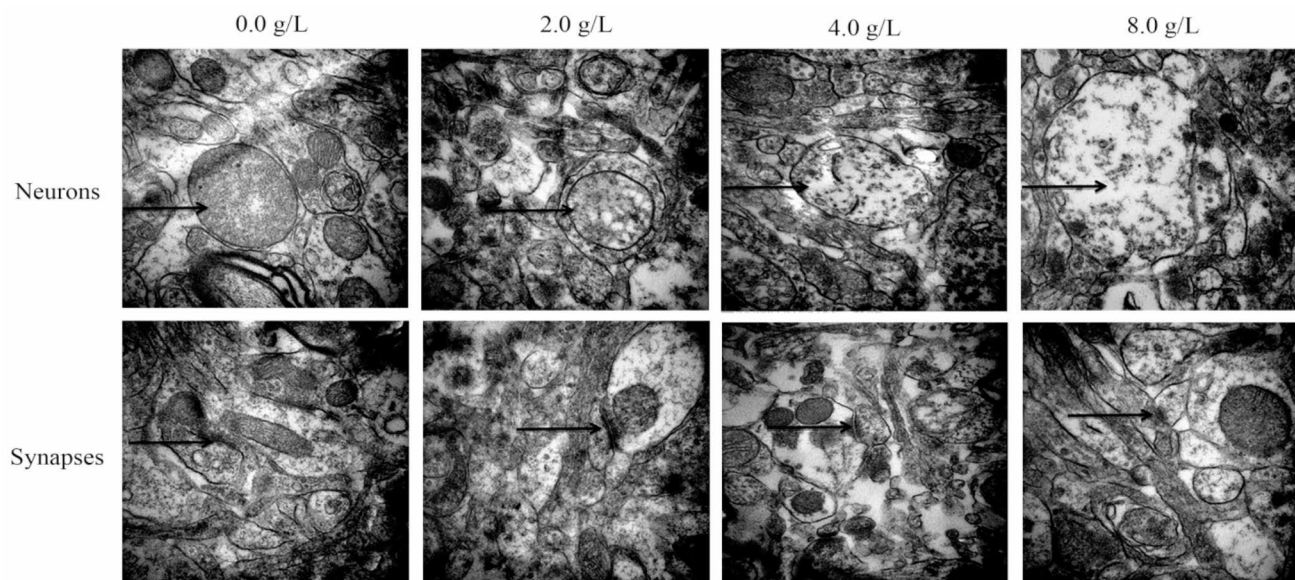


**Fig. 6** Ultrastructure of neurons and synapses in hippocampal CA3 region of rats in each group (50000X)

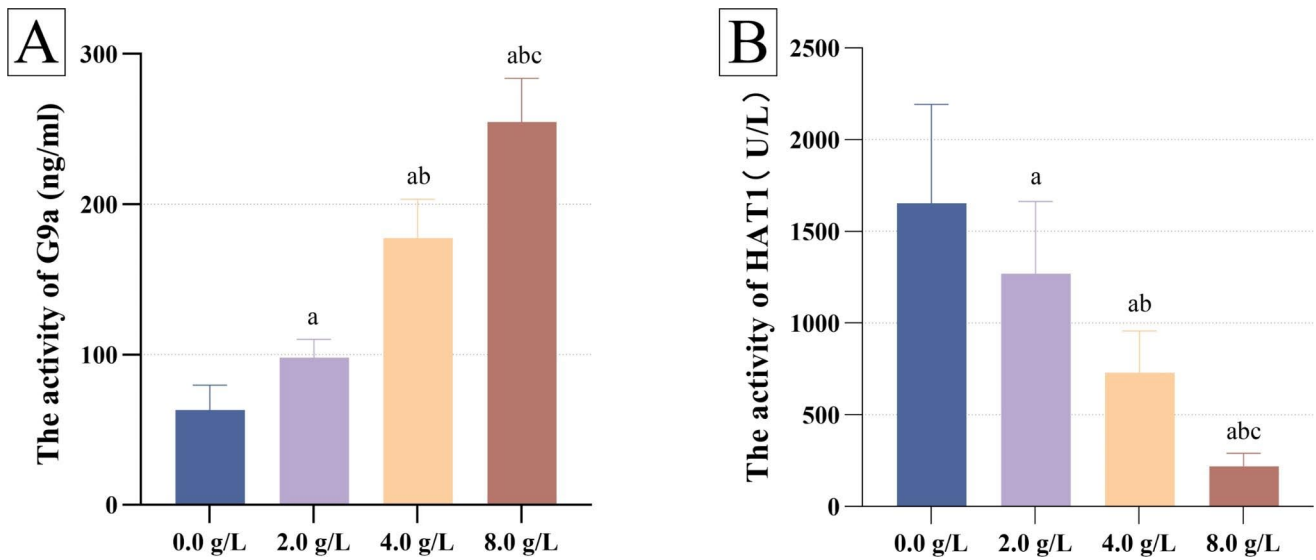
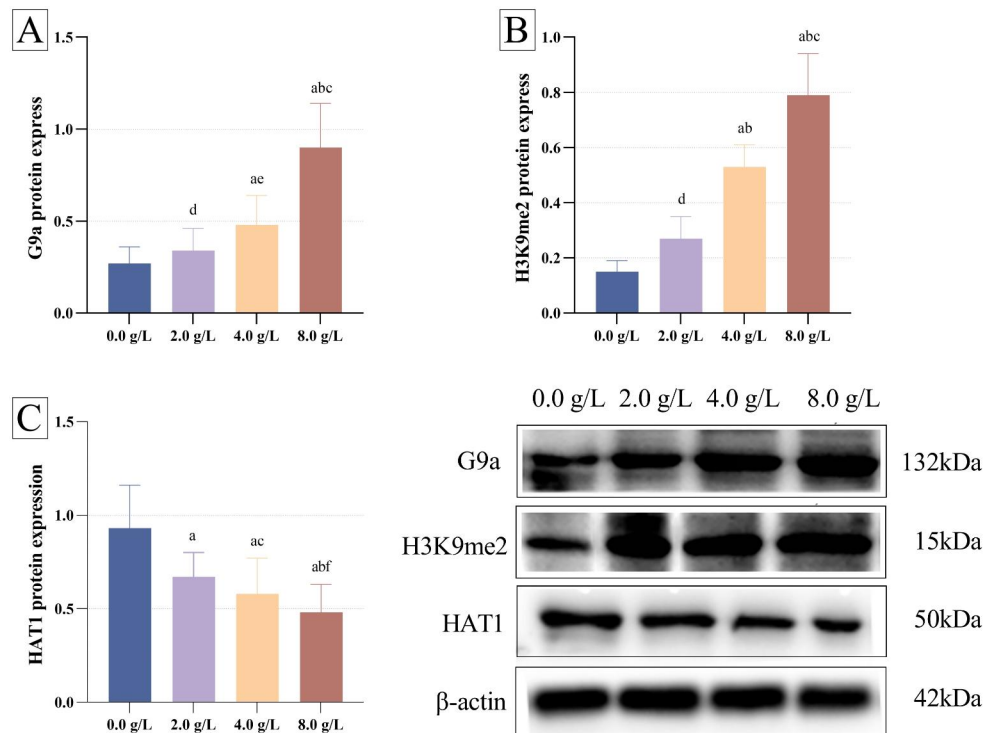


**Fig. 7** Enzyme activity of HAT1 and G9a in rat hippocampus (One-way ANOVA, n=8). Note: <sup>a</sup>*P*<0.01 vs. 0.0 g/L; <sup>b</sup>*P*<0.01 vs. 2.0 g/L; <sup>c</sup>*P*<0.01 vs. 4.0 g/L

**Fig. 8** Protein expression of HAT1, G9a, H3K9me2 in rat hippocampus (One-way ANOVA, n=8). Note: <sup>a</sup>*P*<0.01 vs. 0.0 g/L; <sup>b</sup>*P*<0.05 vs. 2.0 g/L; <sup>c</sup>*P*<0.01 vs. 2.0 g/L; <sup>d</sup>*P*>0.05 vs. 0.0 g/L; <sup>e</sup>*P*>0.05 vs. 2.0 g/L; <sup>f</sup>*P*>0.05 vs. 4.0 g/L



### Changes of Acetylated Histone H3 Protein Expression

Acetylated histone H3 protein expression in the CA3 region of the rat hippocampus was detected using immunohistochemistry, and the results were expressed as AOD and IOD in Fig. 9. It can be roughly observed from the staining situation in Fig. 10 that histone H3 is mainly distributed in the cytoplasm of neurons in rat hippocampal tissue, and

the positive cells show brown or brown-colored cells with increased or deepened staining areas. With the increase of dose, the expression of histone H3 in positive cells decreased gradually, and the brown area became smaller and the color became lighter. The AOD and IOD values of acetylated histone H3 protein expression decreased sequentially in each dosage group ( $F=42.31, P<0.05$ ;  $F=41.12, P<0.05$ ). There was a negative correlation between the AOD and IOD values of acetylated histone H3 protein expression and the

**Fig. 9** Expression of acetylated histone H3 in hippocampal CA3 region of rats in each group.

Note: <sup>a</sup> $P < 0.01$  vs. 0.0 g/L; <sup>b</sup> $P < 0.01$  vs. 2.0 g/L; <sup>c</sup> $P < 0.01$  vs. 4.0 g/L; <sup>d</sup> $P > 0.05$  vs. 2.0 g/L; <sup>e</sup> $P > 0.05$  vs. 4.0 g/L

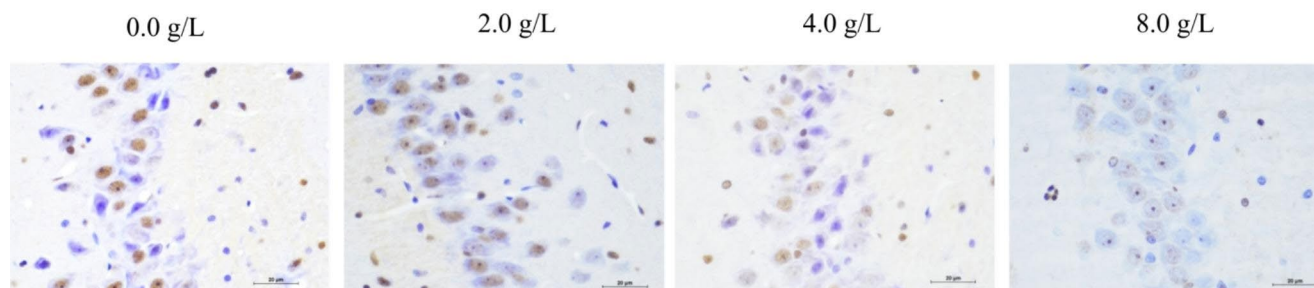
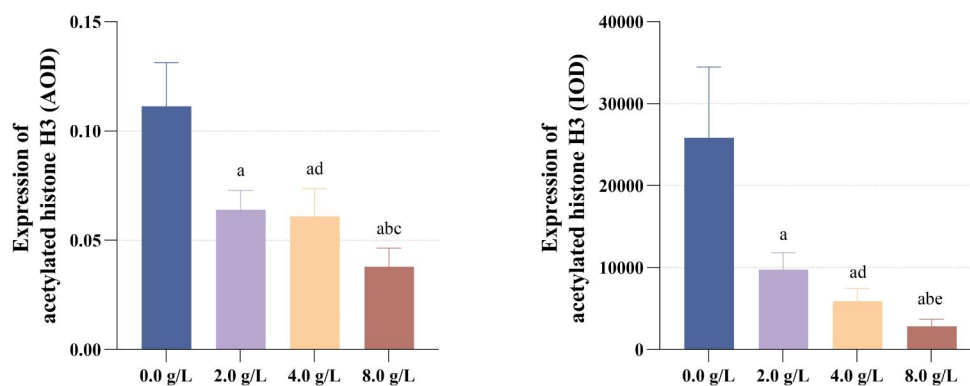


**Fig. 10** Representative immunohistochemical micrographs of acetylated histone H3 in the CA3 region of rats (40X)

dosage of Al, respectively ( $r = -0.77$ ,  $P < 0.05$ ;  $r = -0.87$ ,  $P < 0.05$ ).

## Discussion

Al is the most abundant metallic element in the earth's crust [16], which widely exists in all aspects of production and life. It enters the human body through various ways and accumulates in brain tissue, thus causing neurotoxicity to the human body [17]. The results of MWM experiment in this study showed that the escape latency of rats exposed to subchronic Al was prolonged, and the time of staying in the target quadrant and the number of crossing the platform were shortened, indicating that AlCl<sub>3</sub> impaired the spatial learning and spatial memory ability of rats.

The core of the neurotoxicity of Al is the decreased ability of learning and memory, and the neurobiological basis of learning and memory is synaptic plasticity. Synaptic plasticity refers to the characteristics or phenomena that the morphology and function of synapses can undergo relatively lasting changes, including structural and functional plasticity [18, 19]. This study showed that the arrangement of nerve fibers in the hippocampus of rats exposed to Al was irregular, and the dislocation and loss of nerve cells even appeared vacuole-like changes, and the above changes showed a dose-response relationship with Al exposure dose. Therefore, we speculate that the learning and memory

function of rats injured by Al may be related to the damage of rat hippocampal nerve cells by Al exposure, thus weakening the synaptic transmission efficiency and/or changing the synaptic biological characteristics. This speculation is consistent with relevant reports [13].

Epigenetic modifications are associated with neurodegeneration and cognitive decline, and dysregulation of transcriptional activity leads to abnormal neuronal function [20, 21]. Currently, histone acetylation and methylation markers have been found to be associated with aging and cognitive function [22–24]. For example, memory impairments in the brains of aging mice have been associated with dysacetylation of histones during learning and failure to activate hippocampal gene expression programs which are associated with memory consolidation [25]. HDACs act to deacetylate and can damage cognitive performance in AD models [26] and in aged mice [25]. It has been shown that downregulation of acetyltransferase inhibitors levels in mice with AD models increases histone acetylation levels, thereby restoring synaptic plasticity and learning memory functions and attenuating tau protein phosphorylation and  $\beta$ -amyloid aggregation in AD mice [27]. This conclusion is consistent with the conclusion of this study, Al exposure can inhibit histone H3 acetylation by reducing HAT1 activity and protein expression, and ultimately lead to learning and memory damage.

The histone H3K4me3 and H3K4-specific histone methyltransferase MLL2 are necessary for long-term memory

formation [28, 29]. Histone H3K9me2 and H3K9me2-specific histone methyltransferase EHMT1/2 are associated with memory consolidation [30], and postnatal EHMT1/2 neuron-specific defects lead to learning and environmental adaptation deficits [31]. Recent evidence suggests that G9a is a target for AD because its epigenetic marks are linked to transcription of genes that inhibit learning and memory formation, which leads to cognitive impairment [20, 32, 33]. According to one study, the histone acetylation and methylation processes are regulated by the chromatin-modifying enzymes CBP and G9a, which may serve as epigenetic regulators of memory formation processes [34]. H3K9me2 is a known marker of gene transcriptional silencing. Studies have proved that long-term exposure to AI may inhibit PHF8 and prevent its function as a demethylase, which may block the demethylation of H3K9me2, reduce the expression of BDNF protein, lead to LTP damage, and affect learning and memory. From the perspective of methyltransferase, this study discovered that the expression and activity of G9a protein in the AI-treated groups were higher than those in 0.0 g/L group, and the expression level of H3K9me2 protein in all AI-treated groups was higher than that in 0.0 g/L group, indicating that subchronic AI exposure increased the level of methylated histone H3 in the hippocampus of rats, which was consistent with the existing relevant reports and conclusions [35].

In addition, this study found that AI exposure decreased the acetylation level of histone H3 and increased the level of dimethylated histone H3K9 simultaneously, which affects learning and memory ability. However, the association between histone acetylation and histone methylation in the mechanism of neurotoxicity induced by AI needs further study. In conclusion, the changes of epigenetic indexes such as histone acetylation and methylation in rat hippocampus are one of the significant mechanisms of learning and memory damage in rats induced by AI.

**Acknowledgements** We would like to thank Dr. Lifeng Zhang for reading and editing of the manuscript thoroughly.

**Author Contributions** Author Contribution J.G, W.L and J.L designed and conducted the research; N.H and J.P performed the experiments; J.G and W.L analyzed the data and wrote the paper; J.G, W.L and L.Z reviewed and edited the manuscript. All authors edited and approved the final manuscript.

**Funding** This study is supported by grants from National Natural Science Foundation of China (81673226); Initiated Research Foundation for the Doctoral Program of Science and Technology Department of Liaoning Province, China (201601226); Natural Science Foundation of Education Department of Liaoning Province, China (L2015544, LJKZ1146); Natural Science Foundation for Innovation and Entrepreneurship Training Program of Education Department of Liaoning Province, China (201710164000038); Natural Science Foundation of Science and Technology Department of Shenyang City, China (17-231-1-44); Natural Science Foundation of Shenyang Medical College,

China (20153043); Natural Science Foundation for graduate students of Shenyang Medical College, China (Y20180512); Natural Science Foundation for undergraduate students of Shenyang Medical College, China (20179028).

**Data Availability** This published article and its supplemental information file contain all data created or analyzed throughout this experiment.

## Declarations

**Competing interests** The authors declare no competing interests.

**Ethics approval and consent to participate** All animal experiments were conducted in accordance with the ethical review protocol approved in advance by Shenyang Medical College.

**Consent for Publication** All authors have read and approved the manuscript for submission.

## References

1. Klotz K, Weistenhöfer W, Neff F et al (2017) The Health effects of Aluminum exposure. *Dtsch Arztebl Int* 114(39):653–659. <https://doi.org/10.3238/arztebl.2017.0653>
2. Masson JD, Angrand L, Badran G et al (2022) Clearance, bio-distribution, and neuromodulatory effects of aluminum-based adjuvants. Systematic review and meta-analysis: what do we learn from animal studies? *Crit Rev Toxicol* 52(6):403–419. <https://doi.org/10.1080/10408444.2022.2105688>
3. Rahimzadeh MR, Rahimzadeh MR, Kazemi S et al (2022) Aluminum Poisoning with emphasis on its mechanism and treatment of intoxication. *Emerg Med Int* 2022:1480553. <https://doi.org/10.1155/2022/1480553>
4. Liaquat L, Sadir S, Batool Z et al (2019) Acute aluminum chloride toxicity revisited: study on DNA damage and histopathological, biochemical and neurochemical alterations in rat brain. *Life Sci* 217:202–211. <https://doi.org/10.1016/j.lfs.2018.12.009>
5. Hayashi Y (2022) Molecular mechanism of hippocampal long-term potentiation-towards multiscale understanding of learning and memory. *Neurosci Res* 175:3–15. <https://doi.org/10.1016/j.neures.2021.08.001>
6. Liu W, Liu J, Gao J et al (2022) Effects of Subchronic Aluminum exposure on Learning, Memory, and neurotrophic factors in rats. *Neurotox Res* 40(6):2046–2060. <https://doi.org/10.1007/s12640-022-00599-z>
7. Fogwe LA, Reddy V, Mesfin FB, Neuroanatomy (2023) Hippocampus. *StatPearls*. Treasure Island (FL), vol 20. StatPearls Publishing
8. Lin X, Amalraj M, Blanton C et al (2021) Noncanonical projections to the hippocampal CA3 regulate spatial learning and memory by modulating the feedforward hippocampal trisynaptic pathway. *PLoS Biol* 19(12):e3001127 Published 2021 Dec 20. <https://doi.org/10.1371/journal.pbio.3001127>
9. Ikram MF, Farhat SM, Mahboob A et al (2021) Expression of DnMTs and MBDS in AIC13-Induced Neurotoxicity Mouse Model. *Biol Trace Elem Res* 199(9):3433–3444. <https://doi.org/10.1007/s12011-020-02474-4>
10. Wang F, Kang P, Li Z et al (2019) Role of MLL in the modification of H3K4me3 in aluminium-induced cognitive dysfunction. *Chemosphere* 232:121–129. <https://doi.org/10.1016/j.chemosphere.2019.05.099>

11. Wang J, Feng S, Zhang Q et al (2023) Roles of histone acetyltransferases and deacetylases in the Retinal Development and Diseases. *Mol Neurobiol* 60(4):2330–2354. <https://doi.org/10.1007/s12035-023-03213-1>
12. Sanaei M, Kavooosi F (2021) Histone deacetylase inhibitors, intrinsic and extrinsic apoptotic pathways, and epigenetic alterations of Histone Deacetylases (HDACs) in Hepatocellular Carcinoma. *Iran J Pharm Res* 20(3):324–336. <https://doi.org/10.22037/ijpr.2021.115105>
13. Gao J, Zhang S, Li B et al (2023) Sub-chronic aluminum exposure in rats' learning-memory capability and hippocampal histone H4 acetylation modification: effects and mechanisms [published online ahead of print, 2023 Feb 24]. *Biol Trace Elem Res*. <https://doi.org/10.1007/s12011-023-03602-6>
14. Butler AA, Johnston DR, Kaur S et al (2019) Long noncoding RNA NEAT1 mediates neuronal histone methylation and age-related memory impairment. *Sci Signal* 12(588):eaaw9277 Published 2019 Jul 2. <https://doi.org/10.1126/scisignal.aaw9277>
15. Griñán-Ferré C, Marsal-García L, Bellver-Sanchis A et al (2019) Pharmacological inhibition of G9a/GLP restores cognition and reduces oxidative stress, neuroinflammation and  $\beta$ -Amyloid plaques in an early-onset Alzheimer's Disease mouse model. *Aging* 11(23):11591–11608. <https://doi.org/10.18632/aging.102558>
16. Jeong CH, Kwon HC, Kim DH et al (2020) Effects of Aluminum on the Integrity of the intestinal epithelium: an in Vitro and in vivo study. *Environ Health Perspect* 128(1):17013. <https://doi.org/10.1289/ehp5701>
17. Hosseini SM, Hejazian LB, Amani R et al (2020) Geraniol attenuates oxidative stress, bioaccumulation, serological and histopathological changes during aluminum chloride-hepatopancreatic toxicity in male Wistar rats. *Environ Sci Pollut Res Int* 27(16):20076–20089. <https://doi.org/10.1007/s11356-020-08128-1>
18. Nguyen PV, Connor SA (2019) Noradrenergic regulation of Hippocampus-Dependent memory. *Cent Nerv Syst Agents Med Chem* 19(3):187–196. <https://doi.org/10.2174/1871524919666190719163632>
19. Joshi VV, Patel ND, Rehan MA, Kuppa A (2019) Mysterious mechanisms of memory formation: are the answers hidden in synapses? *Cureus*. 11(9):e5795. <https://doi.org/10.7759/cureus.5795>
20. Griñán-Ferré C, Corpas R, Puigoriol-Illamola D et al (2018) Understanding epigenetics in the neurodegeneration of Alzheimer's Disease: SAMP8 mouse model. *J Alzheimers Dis* 62(3):943–963. <https://doi.org/10.3233/jad-170664>
21. Harman MF, Martin MG (2020) Epigenetic mechanisms related to cognitive decline during aging. *J Neurosci Res* 98(2):234–246. <https://doi.org/10.1002/jnr.24436>
22. Fischer A, Sananbenesi F, Mungenast A, Tsai LH (2010) Targeting the correct HDAC(s) to treat cognitive disorders. *Trends Pharmacol Sci* 31(12):605–617. <https://doi.org/10.1016/j.tips.2010.09.003>
23. Gräff J, Tsai LH (2013) The potential of HDAC inhibitors as cognitive enhancers. *Annu Rev Pharmacol Toxicol* 53:311–330. <https://doi.org/10.1146/annurev-pharmtox-011112-140>
24. Greer EL, Shi Y (2012) Histone methylation: a dynamic mark in health, Disease and inheritance. *Nat Rev Genet* 13(5):343–357. <https://doi.org/10.1038/nrg3173>
25. Peleg S, Sananbenesi F, Zovoilis A et al (2010) Altered histone acetylation is associated with age-dependent memory impairment in mice [published correction appears in *Science*. ;328(5986):1634]. *Science*. 2010;328(5979):753–756. <https://doi.org/10.1126/science.1186088>
26. Gräff J, Rei D, Guan JS et al (2012) An epigenetic blockade of cognitive functions in the neurodegenerating brain. *Nature* 483(7388):222–226 Published 2012 Feb 29. <https://doi.org/10.1038/nature10849>
27. Chai GS, Feng Q, Wang ZH et al (2017) Downregulating ANP32A rescues synapse and memory loss via chromatin remodeling in Alzheimer model. *Mol Neurodegener* 12(1):34 Published 2017 May 4. <https://doi.org/10.1186/s13024-017-0178-8>
28. Gupta S, Kim SY, Artis S et al (2010) Histone methylation regulates memory formation. *J Neurosci* 30(10):3589–3599. <https://doi.org/10.1523/jneurosci.3732-09.2010>
29. Kerimoglu C, Agis-Balboa RC, Kranz A et al (2013) Histone-methyltransferase MLL2 (KMT2B) is required for memory formation in mice [published correction appears in *J Neurosci*. ;33(16):7108]. *J Neurosci*. 2013;33(8):3452–3464. <https://doi.org/10.1523/jneurosci.3356-12.2013>
30. Gupta-Agarwal S, Franklin AV, Deramus T et al (2012) G9a/GLP histone lysine dimethyltransferase complex activity in the hippocampus and the entorhinal cortex is required for gene activation and silencing during memory consolidation. *J Neurosci* 32(16):5440–5453. <https://doi.org/10.1523/jneurosci.0147-12.2012>
31. Schaefer A, Sampath SC, Intrator A et al (2009) Control of cognition and adaptive behavior by the GLP/G9a epigenetic suppressor complex. *Neuron* 64(5):678–691. <https://doi.org/10.1016/j.neuron.2009.11.019>
32. Zheng Y, Liu A, Wang ZJ et al (2019) Inhibition of EHMT1/2 rescues synaptic and cognitive functions for Alzheimer's Disease. *Brain* 142(3):787–807. <https://doi.org/10.1093/brain/awy354>
33. Han JLT, Pang KKL, Ang SRX et al (2021) Inhibition of lysine methyltransferase G9a/GLP reinstates long-term synaptic plasticity and synaptic tagging/capture by facilitating protein synthesis in the hippocampal CA1 area of APP/PS1 mouse model of Alzheimer's Disease. *Transl Neurodegener* 10(1):23 Published 2021 Jun 29. <https://doi.org/10.1186/s40035-021-00247-0>
34. Subbanna S, Joshi V, Basavarajappa BS (2018) Activity-dependent signaling and Epigenetic Abnormalities in mice exposed to postnatal ethanol. *Neuroscience* 392:230–240. <https://doi.org/10.1016/j.neuroscience.2018.07.011>
35. Li H, Xue X, Li Z et al (2020) Aluminium-induced synaptic plasticity injury via the PHF8-H3K9me2-BDNF signalling pathway. *Chemosphere* 244:125445. <https://doi.org/10.1016/j.chemosphere.2019.125445>

**Publisher's Note** Springer Nature remains neutral with regard to jurisdictional claims in published maps and institutional affiliations.

Springer Nature or its licensor (e.g. a society or other partner) holds exclusive rights to this article under a publishing agreement with the author(s) or other rightsholder(s); author self-archiving of the accepted manuscript version of this article is solely governed by the terms of such publishing agreement and applicable law.